Supplemental material to "Spin relaxation mechanism in graphene: resonant scattering by magnetic impurities."

Denis Kochan, Martin Gmitra, and Jaroslav Fabian
Institute for Theoretical Physics, University of Regensburg, 93040 Regensburg, Germany

Details to first-principles calculations.

Density functional theory [1] has been used to calculate the electronic structure of hydrogenated graphene in the supercell approach. We used the generalized gradient approximation for the exchange-correlation functional [2]. The atomic positions in the supercell calculations have been relaxed using the quasi-newton algorithm based on the trust radius procedure implemented within the plane wave pseudopotential code Quantum ESPRESSO [3]. For the atomic species we have used ultra-soft pseudopotentials [4, 5] with PBE exchange-correlation functional [2] with kinetic energies cut-offs of 30 Ry for the wave function and 300 Ry for the density. The vacuum of 15 Å to separate the hydrogenated graphene planes has been used. We found that the covalent C-H bond length d_{H} is close to 1.13 Å. Next-nearest distance a between the three closest carbon atoms to the hydrogenated carbon, a tetrahedral edge length, is 2.516 Å. The hydrogen bonding distorts the graphene plane by pulling the hydrogenated carbon atom out of plane by about 0.36 Å.

The relaxed structure was then used in the full-potential spin-polarized self-consistent calculations using the linearized augmented plane wave (FLAPW) method as implemented in the FLEUR code [6] in the film mode. We used the cut-off parameter for the plane wave-expansion $\mathrm{k}_{\max} = 4.7\ \mathrm{bohr}^{-1}$ and 64 k-points in the irreducible wedge of the Brillouin zone. The muffin-tin radii for carbon of 1.32 bohr and for hydrogen 0.81 bohr were used.

Spin-polarized band structure of hydrogenated graphene.

The electronic structure of a relaxed 5×5 supercell with a single H atom on top of a C atom (denoted below as $\mathrm{C_H}$) has been calculated using the FLEUR code [6]. Figure 1(a-f) shows the results. The valence and conduction bands are separated at K point due to covalent bonding of carbon p_z and hydrogen s orbitals by about 1 eV. In between lies the mid-gap band formed mainly by p_z orbitals of C atoms closest to H. The ground state is ferrimagnetic, for details see Fig. 1(c-e). The magnetic moment is significant in a close neighborhood of $\mathrm{C_H}$ only, oscillating as a function of position. The largest moment, of 0.054 μ_{B}, is on the nearest neighbors to $\mathrm{C_H}$. Hence the spin splitting of the mid-gap states is maximal and gradually decreases for the bands away from the Fermi level, whose character is less influenced by the H. Employing criterion for the formation of magnetic moment [7], we conclude that hydrogen adatom on graphene creates a stable magnetic moments formation. In supercell calculations, however, these magnetic moments are periodically repeated, which can lead to an artificial coupling due to long-range interactions [7, 8]. Defect induced magnetism on graphene and its underlying magnetic texture are in focus of intensive discussion [9–14]. We note that particular magnetic ordering for the present study is not inevitable.

To parameterize the first-principles data, we have extended the hopping Hamiltonian studied in Refs. [15–17]. The scheme is in Fig. 1(g). The orbital effects due to H are captured by on-site energy ε_{h} and hopping T. To this we add local Zeeman couplings J_{h}, J_1 and J_2, on the sites of large magnetic moments, inspired by Fig. 1(f). The impurity Hamiltonian H'_{eff}, which is added to graphene's $H_0 = -t\sum_{\langle m,n\rangle} c_m^\dagger c_n$ ($t = 2.6\,\mathrm{eV}$) is

$$H'_{\mathrm{eff}} = \sum_\sigma h_\sigma^\dagger(\varepsilon_{\mathrm{h}} - J_{\mathrm{h}}\sigma)h_\sigma + T(h_\sigma^\dagger c_{\mathrm{C_H},\sigma} + c_{\mathrm{C_H},\sigma}^\dagger h_\sigma) - J_1\sum_{m_1,\sigma}\sigma\, c_{m_1,\sigma}^\dagger c_{m_1,\sigma} - J_2\sum_{m_2,\sigma}\sigma\, c_{m_2,\sigma}^\dagger c_{m_2,\sigma}\,. \tag{1}$$

Here $h_\sigma^\dagger$ (h_σ) and $c_\sigma^\dagger$ (c_σ) are fermionic creation (annihilation) operators acting on the hydrogen and graphene carbon sites, respectively. Subscript $\sigma = \{\uparrow,\downarrow\} = \{+1,-1\}$ stands for the spin component along the z-direction (quantization axis). Subscripts m_1 and m_2 label the three first-nearest and the six second-nearest neighbors of $\mathrm{C_H}$.

Orbital parameters $\varepsilon_{\mathrm{h}} = 0.16\,\mathrm{eV}$ and $T = 7.5\,\mathrm{eV}$ were fitted already in Ref. [17]. Least-square fitting the model Hamiltonian H'_{eff}, Eq. (1), to our supercell spin-polarized first-principles data, gives $J_{\mathrm{h}} = -0.82\,\mathrm{eV}$, $J_1 = 0.69\,\mathrm{eV}$, and $J_2 = -0.18\,\mathrm{eV}$. We fitted the valence, mid-gap, and conduction bands at 100 equidistant points along $\Gamma - \mathrm{K} - \mathrm{M} - \Gamma$ lines in Brillouin zone. The fits, shown in Fig. 1(a) and detailed in Fig. 1(c-e), are remarkably good especially around K. We find that J_{h} alone controls the exchange splitting of the valence and conduction bands in a large region around K point.

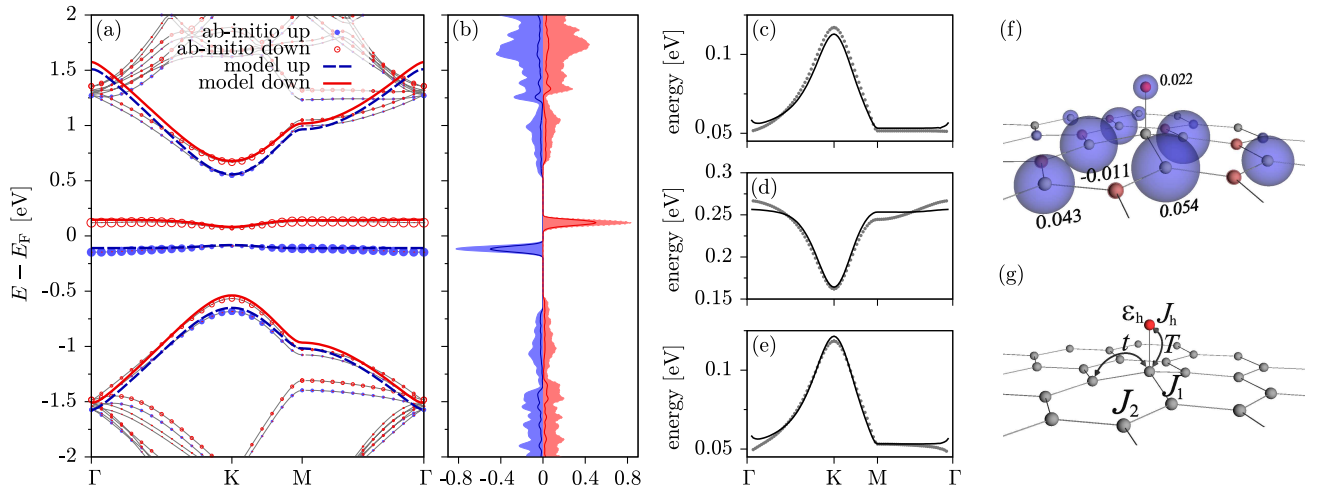

FIG. 1. First-principles results for a 5×5 graphene supercell with a single hydrogen adatom. (a) Spin-polarized band structure. The circles radii indicate the presence of p_z orbitals from the nearest neighbors to C_H. Bold lines (dashed and solid) come from the exchange hopping model, Eq. (1). (b) Total density of states per atom (filled) and p_z projected local densities summed up to the third nearest carbon atoms to C_H, normalized to the corresponding number of atoms in the set. Exchange splittings of the conduction (c), mid-gap (d), and valence (e) bands. Solid lines are from the model. (f) Local magnetic moments around hydrogen, indicated in μ_B. (g) Exchange hopping model of Eq. (1).

Spin relaxation rate.

The spin relaxation rate is obtained by formulating rate equations. Suppose we have an electron spin accumulation in graphene described by the spin (σ)-dependent chemical potential μ_σ. The electron distribution functions differ from equilibrium as $f_{k\sigma} = f^0_k + \delta f_{k\sigma}$, where

$$\delta f_{k\sigma} \approx \left(-\frac{\partial f^0_k}{\partial \varepsilon_k}\right)(\mu_\sigma - \varepsilon_F). \tag{2}$$

We denoted as $f^0_k = f^0(\varepsilon_k)$ the Fermi-Dirac function, ε_k the electron energy, and ε_F the Fermi level. The electron spin is

$$s = \sum_k \left(-\frac{\partial f^0_k}{\partial \varepsilon_k}\right)\mu_s, \tag{3}$$

with $\mu_s = \mu_\uparrow - \mu_\downarrow$. The spin relaxation rate is defined from equation,

$$\frac{\partial s}{\partial t} = \sum_k \left(-\frac{\partial f^0_k}{\partial \varepsilon_k}\right)\frac{\partial \mu_s}{\partial t} \equiv -\frac{s}{\tau_s}. \tag{4}$$

Let $W_{k\uparrow\Downarrow|k'\downarrow\Uparrow}$ be the spin-flip rate, that is, the rate of the transition of an electron with momentum k and spin up ($\uparrow$), in the presence of an impurity with spin down ($\Downarrow$), to another state of momentum k' and spin down ($\downarrow$), and impurity spin up ($\Uparrow$) (the electron and impurity spins are flipped). Let the probability of the impurity spin being $\Sigma = \{\Uparrow, \Downarrow\}$ be p_Σ. The rate equation for spin up electrons is

$$\begin{aligned}\frac{\partial f_{k\uparrow}}{\partial t} = &-\sum_{k'} W_{k\uparrow\Downarrow|k'\downarrow\Uparrow}\; p_\Downarrow f_{k\uparrow}\,(1 - f_{k'\downarrow}) \\ &+\sum_{k'} W_{k'\downarrow\Uparrow|k\uparrow\Downarrow}\; p_\Uparrow f_{k'\downarrow}\,(1 - f_{k\uparrow})\,.\end{aligned} \tag{5}$$

Assuming unpolarized magnetic moments, $p_\Uparrow = p_\Downarrow = 1/2$, and using the symmetry of the spin-flip rates, we get

$$\frac{\partial f_{k\uparrow}}{\partial t} = -\frac{1}{2}\sum_{k'} W_{k\uparrow\Downarrow|k'\downarrow\Uparrow}\,(f_{k\uparrow} - f_{k'\downarrow})\,. \tag{6}$$

Similarly for the rate of $f_{k\downarrow}$. We can then write

$$\frac{\partial s}{\partial t} = -\sum_k \sum_{k'} W_{k\uparrow\Downarrow|k'\downarrow\Uparrow}\,(\delta f_{k\uparrow} - \delta f_{k'\downarrow})\,. \tag{7}$$

Substituting the spin accumulation and comparing with the defining equation for τ_s we get

$$\frac{1}{\tau_s} = \frac{\sum_k \sum_{k'} \left(-\partial f^0_k/\partial \varepsilon_k\right) W_{k\uparrow\Downarrow|k'\downarrow\Uparrow}}{\sum_k \left(-\partial f^0_k/\partial \varepsilon_k\right)}. \tag{8}$$

This equation is used to evaluate the temperature-dependent spin relaxation rates in the paper.

Finally, the transition rates in the presence of N_H impurities are calculated from the T-matrix,

$$W_{k\sigma\Sigma|k'\sigma'\Sigma'} = N_H \tfrac{2\pi}{\hbar}\left|T_{k\sigma\Sigma|k'\sigma'\Sigma'}\right|^2 \delta(\varepsilon_k - \varepsilon_{k'}). \tag{9}$$

All what is necessary for spin-flip rates is to transform the singlet and triplet T-matrix amplitudes, Eq. (4) in the paper, via composite spin states $|\uparrow,\Downarrow\rangle$ and $|\downarrow,\Uparrow\rangle$. This is a place where the function $f_{\sigma,\sigma'}(x,y)$, Eq. (7) in the main text, enters the game.

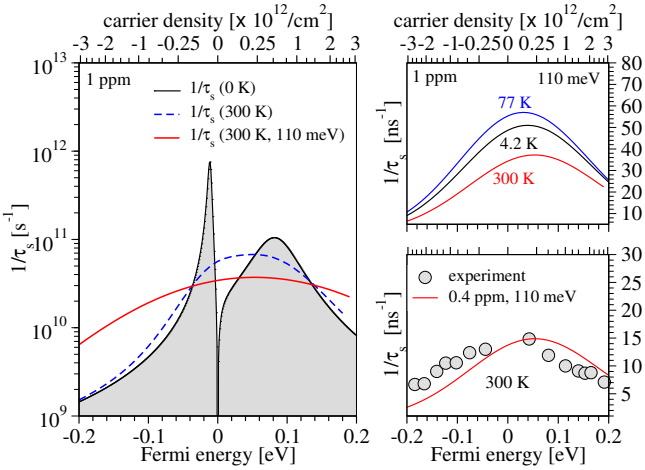

FIG. 2. Same as Fig. 1 of the paper, but with $J = 0.4$ eV. (a) Spin relaxation rate $1/\tau_s$ at zero temperature, at 300 K, and at 300 K and broadened by puddles with 110 meV Dirac point fluctuations. The rates are plotted as functions of energy and (top scale) electron density. The impurity concentration is 1 ppm. (b) Spin relaxation rates, broadened by puddles, at different temperatures. (c) Comparison with experiment, for 0.4 ppm of impurities.

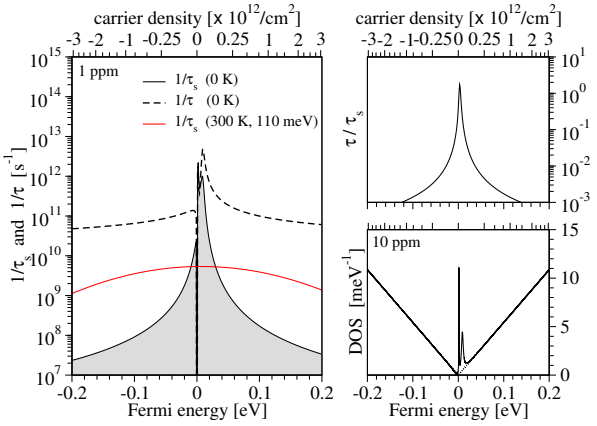

FIG. 3. Spin relaxation rate for $J = -0.04$ eV. (a) Spin relaxation $1/\tau_s$ and spin-preserving $1/\tau$ rates as functions of energy and electron density (top scale). The spin relaxation rate is also shown at 300 K and broadened by puddles with 110 eV energy broadening. The calculations are for 1 ppm impurities. (b) The ratio of the spin-flip and spin-preserving rates. (c) Density of states for 10 ppm of impurities.

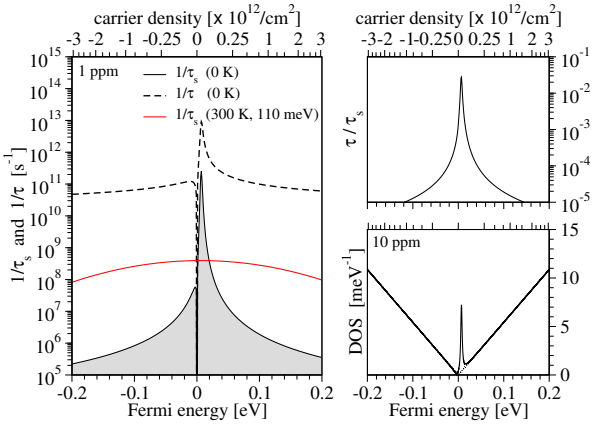

FIG. 4. Same as in Fig. 3 but for $J = -0.004$ eV.

Robustness of spin flip resonant scattering.

In Fig. 2 we show the results for the spin relaxation rates for a ferromagnetic coupling of $J = 0.4$ eV. The singlet and triplet peaks are flipped relative to Fig. 1 of the paper, which is for the antiferromagnetic coupling. Although in a clean system at low temperatures the peaks could be observed, the presence of puddles (or different types of magnetic impurities) wash out the peak structure. Apart a minor detail the results are quantitatively similar to the antiferromagnetic case, namely, the averaged spin relaxation rate is skewed towards positive energies, reflecting the flipped singlet and triplet peaks.

In the paper we claim that the spin relaxation rate is not sensitive to the precise value of J as long as $|J| \gtrsim \Gamma$, where Γ is the resonance width. In Figs. 3, 4, and 5, we plot $1/\tau_s$ and spin-preserving rate $1/\tau$ for exchange couplings $J = -0.04$ eV, $J = -0.004$ eV, and $J = -0.0004$ eV. For $J = -0.04$ eV, the spin relaxation rate for 1 ppm of impurities is still about 100 ps, since at resonance the value of $1/\tau_s$ is unchanged (compared to $J = -0.4$ eV). This lower value of J could also be used to explain the experiment! The singlet and triplet peaks are still resolved. In Fig. 3(b) we plot the ratio of the spin-flip to spin-conserving rates. At resonances, this ratio is about one, meaning that we are still in the regime of $J \gtrsim \Gamma$, and not in the perturbative regime (which is visible outside of the resonance peaks). In Fig. 3(c) we plot the density of states around the Dirac point. The split peak is visible.

If the exchange J further decreases (Γ is of order of 10 meV), although the resonance peaks are present, the spin-flip scattering rates become smaller than the spin-preserving rates, as expected from conventional perturbative (Fermi golden rule) scattering. In particular, it is expected that if $|J| < \Gamma$, the ratio τ/τ_s decreases as J^2 with decreasing J. This is evident in Figs. 4 and 5. *This is also the regime of spin-orbit coupling.* Say, if an adatom induces local spin-orbit coupling of 1 meV, which is reasonable, then resonance scattering would enhance the spin-orbit spin relaxation rate roughly as 1/16 ($1/4^2$) compared to what is shown in Fig. 4 (which is for $|J| = 4$ meV). For a 1 ppm of adatoms the spin relaxation time would be 10-100 nanoseconds. The experimental rates could then be achieved by $\eta \approx 10^{-4} - 10^{-3}$ spin-orbit coupling inducing resonant adatoms.

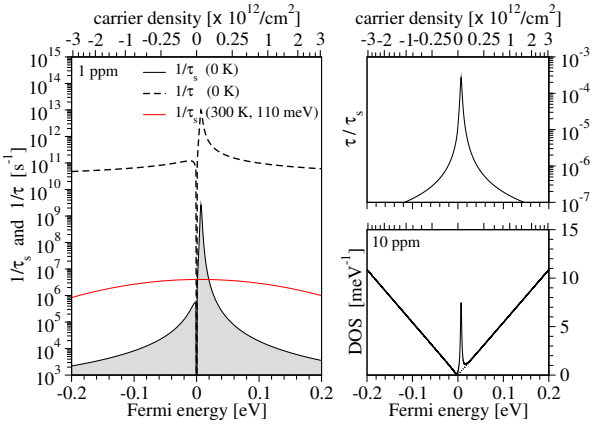

FIG. 5. Same as in Fig. 3 but for $J = -0.0004$ eV.

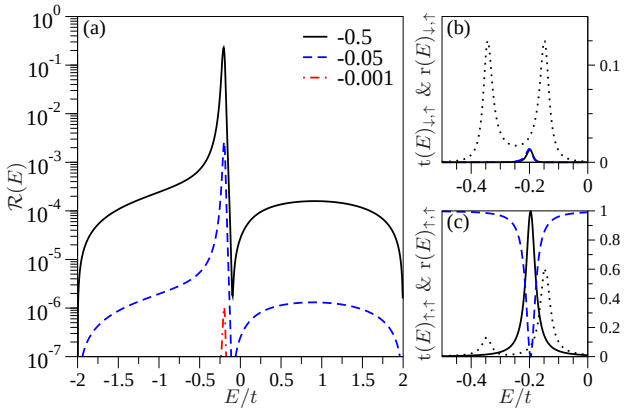

FIG. 6. Atomic chain with a local spin sitting at one of the barriers. (a) Ratio $\mathcal{R}(E)$ of spin-flip versus spin-conserving transition probabilities for $U/t = 10$ and indicated values of J/t. (b) Spin-flip transmission (solid) $\mathrm{t}(E)_{\downarrow,\uparrow}$ and reflection (dashed) $\mathrm{r}(E)_{\downarrow,\uparrow}$ for $J/t = -0.05$, both magnified by factor 10. (c) Same as in panel (b) but for spin-conserving quantities $\mathrm{t}(E)_{\uparrow,\uparrow}$ and $\mathrm{r}(E)_{\uparrow,\uparrow}$. For both panels (b) and (c) the dotted lines on the background show corresponding quantities from the resonant model, Eqs. (11) and (12) in the main paper.

Double-barrier atomic chain with a local moment sitting off the resonant site.

In the paper we state that it is intuitively clear that the exchange coupling on the resonant site dominates spin-flip processes, so we can neglect J on the carbon atoms near hydrogen. We can see this explicitly on our atomic chain model. Suppose a local spin giving exchange J sits not inside resonant well but at one of the barriers, say the left one, i. e. $m = -1$. The model Hamiltonian is as follows:

$$H_{\rm off} = -t \sum_{\langle m,n\rangle} (c_m^\dagger c_n + c_n^\dagger c_m) + \sum_{m=\mp 1} \left(U c_m^\dagger c_m - J\delta_{m,-1}\, \hat{\mathbf{s}}\cdot\hat{\mathbf{S}} \right). \tag{10}$$

Transmissions and reflections amplitudes γ_ℓ and β_ℓ can be calculated to be,

$$\gamma_\ell = \frac{-e^{-ikb} + e^{ikb}\,\mathbb{Y}_\ell}{e^{ikb} + \frac{E_k}{t}(1 + e^{ikb}U/t) + e^{ikb}\,\mathbb{X}_\ell}\,, \tag{11}$$

$$\beta_\ell = \gamma_\ell\,\mathbb{X}_\ell - \mathbb{Y}_\ell\,, \tag{12}$$

where auxiliary functions $\mathbb{X}_\ell$ and $\mathbb{Y}_\ell$ are,

$$\mathbb{X}_\ell = \frac{t + e^{ikb}\,U}{t + e^{ikb}[U - (4\ell - 3)J]}\,, \tag{13}$$

$$\mathbb{Y}_\ell = \frac{t + e^{-ikb}\,[U - (4\ell - 3)J]}{t + e^{+ikb}[U - (4\ell - 3)J]}\,. \tag{14}$$

Figure 6 shows main characteristics of $H_{\rm off}$, Eq. (10), which allows us to call this model as off-resonant. Figure 6(a) provides the ratio $\mathcal{R}(E)$ for spin-flip *versus* spin-conserving probabilities, i. e.,

$$\mathcal{R}(E) = \left[\mathrm{t}(E)_{\sigma,\overline{\sigma}} + \mathrm{r}(E)_{\sigma,\overline{\sigma}}\right] \Big/ \left[\mathrm{t}(E)_{\sigma,\sigma} + \mathrm{r}(E)_{\sigma,\sigma}\right] \tag{15}$$

for different J/t. It is obvious when comparing with Fig. 2(a) in the main text that spin-flip processes are significantly suppressed. Figure 6(b) shows transmission and reflection probabilities $\mathrm{t}(E)_{\downarrow,\uparrow}$ and $\mathrm{r}(E)_{\downarrow,\uparrow}$ for $J/t = -0.05$ (to be visible, they are magnified by factor 10); the dotted line on the background is the transmission probability for the local moment on the resonant site inside the well (see Fig. 2(b) in the main text). Clearly, the spin-flip transitions are much more inhibited than in the resonant case discussed in the paper, justifying neglecting the off-resonant site exchange, especially when energy fluctuations from puddles wash out the fine structure of the resonant peaks. Figure 6(c) shows $\mathrm{t}(E)_{\uparrow,\uparrow}$ (solid line) and $\mathrm{r}(E)_{\uparrow,\uparrow}$ (dashed line) for $J/t = -0.05$. Similarly, the dotted line represents transmission probability $\mathrm{t}(E)_{\uparrow,\uparrow}$ in the resonant case.

[1] J. Hohenberg and W. Kohn, Phys. Rev. **136**, B864 (1964).
[2] J. P. Perdew, K. Burke, and M. Ernzerhof, Phys. Rev. Lett. **77**, 3865 (1996).
[3] P. Giannozzi and et al., J.Phys.: Condens. Matter **21**, 395502 (2009).
[4] D. Vanderbilt, Phys. Rev. B. **41**, 7892 (1990).
[5] Source: `http://www.quantum-espresso.org/wp-content/uploads/upf_files/C.pbe-van_ak.UPF`, `http://www.quantum-espresso.org/wp-content/uploads/upf_files/H.pbe-van_ak.UPF`.
[6] See http://www.flapw.de/.
[7] P. Venezuela, R. B. Muniz, A. T. Costa, D. M. Edwards, S. R. Power, and M. S. Ferreira, Phys. Rev. B **80**, 241413 (2009).
[8] Z. Zanolli and J.-C. Charlier, Phys. Rev. B **81**, 165406 (2010).

[9] O. V. Yazyev and L. Helm, Phys. Rev. B **75**, 125408 (2007).
[10] P. O. Lehtinen, A. S. Foster, Y. Ma, A. V. Krasheninnikov, and R. M. Nieminen, Phys. Rev. Lett. **93**, 187202 (2004).
[11] D. Soriano, N. Leconte, P. Ordejón, J. C. Charlier, J. J. Palacios, and S. Roche, Phys. Rev. Lett. **107**, 016602 (2011).
[12] B. R. K. Nanda, M. Sherafati, Z. Popović, and S. Satpathy, New J. Phys. **14**, 083004 (2012).
[13] M. M. Ugeda, I. Brihuega, F. Guinea, and J. M. Gomez-Rodriguez, Phys. Rev. Lett. **104**, 096804 (2010).
[14] R. R. Nair, M. Sepioni, I. L. Tsai, O. Lehtinen, J. Keinonen, A. V. Krasheninnikov, T. Thomson, A. K. Geim, and I. V. Grigorieva, Nature Physics **8**, 199 (2012).
[15] J. P. Robinson, H. Schomerus, L. Oroszlány, and V. I. Fal'ko, Phys. Rev. Lett. **101**, 196803 (2008).
[16] T. O. Wehling, S. Yuan, A. I. Lichtenstein, A. K. Geim, and M. I. Katsnelson, Phys. Rev. Lett. **105**, 056802 (2010).
[17] M. Gmitra, D. Kochan, and J. Fabian, Phys. Rev. Lett. **110**, 246602 (2013).